Vol. 34 · No. 8 · August 2017

Particle & Particle Systems Characterization

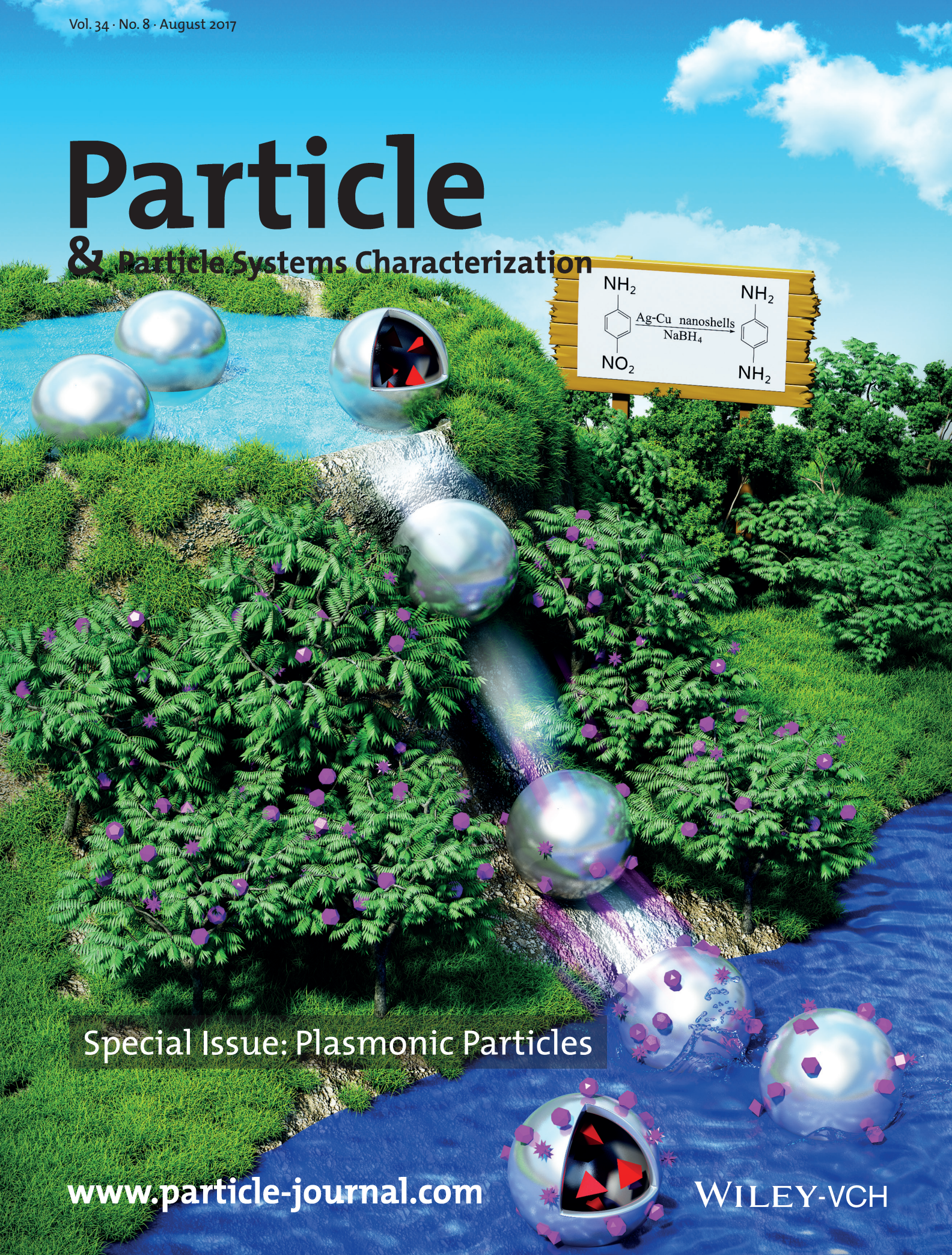

Special Issue: Plasmonic Particles

www.particle-journal.com

WILEY-VCH

Particle & Particle Systems Characterization
www.particle-journal.com

Silver–Copper Hollow Nanoshells as Phase-Transfer Reagents and Catalysts in the Reduction of 4-Nitroaniline

*Limei Chen, Peiguang Hu, Yi Peng, Jia En Lu, Mauricio D. Rojas-Andrade, and Shaowei Chen**

Cysteine-stabilized Ag–Cu hollow nanoshells are prepared by the coreduction of silver nitrate and cupric nitrate with sodium borohydride in the presence of sodium thiocyanate. Transmission electron microscopic measurements show that the resulting Ag–Cu nanoshells exhibit a rather uniform size of 57.2 ± 11.9 nm with a shell thickness of 7.9 ± 1.6 nm, and the hollow volume ratio is estimated to be ≈62%. High-resolution transmission electron microscopic studies show that the nanoshells are composed of nanocrystalline Ag and CuO in segregated domains. Consistent results are obtained in X-ray diffraction measurements. X-ray photoelectron spectroscopic analysis shows that the elemental composition of the nanoshells is consistent with the initial feed ratio of the metal salt precursors. When capped with 1-dodecanethiol, the hollow nanoshells become dispersible in apolar organic solvents and the cavity may be exploited for the effective phase-transfer of target molecules such as rhodamine 6G between water and organic media. The Ag–Cu nanoshells also show apparent catalytic activity toward the reduction of 4-nitroaniline by sodium borohydride, a performance that is markedly better than that of the solid counterparts and comparable to leading results in recent literature based on relevant metal catalysts.

1. Introduction

In recent decades, transition-metal nanostructures such as nanoparticles, nanocubes, nanoplates, and nanoshells have been attracting significant interest largely because of their unique optical and electronic properties and potential applications in diverse fields ranging from catalysis to drug delivery and chemical/biological sensing.[1] Among these, hollow nanoshells represent a unique group of functional nanomaterials, where the materials properties may be deliberately manipulated by the size, shape, shell thickness, and elemental compositions. Furthermore, with proper surface functionalization, the hollow nanoshells may be dispersible in a wide range of solvent media and used for the ready encapsulation and delivery of target molecules.[2] For instance, nanoshells of Pt, Ag, Au, and Au–Ag bimetallic alloys have been prepared, used for drug delivery, and exhibited apparent catalytic activity in a variety of reactions, as compared to their solid counterparts.[3] This is largely ascribed to the high surface area and porous structure of the metal shells that are presumed to facilitate the catalytic reactions and mass transport of reaction species.

Several methods have been reported for the synthesis of hollow metal nanostructures, such as galvanic replacement based on the Kirkendall effect, chemical etching, and rigid templating.[3b,4] With a rigid template, a thin shell structure can be easily formed and tuned; however, final removal of the template is challenging.[5] In the Kirkendall method, a shell is formed via chemical reactions based on a self-template process, by which the template diminishes with the formation of a hollow structure.[6] For instance, Kado et al. reported a simple, one-pot synthesis of silver nanoshells based on nanoscale Kirkendall effect by the sequential addition of NaSCN and $NaBH_4$ into an $AgNO_3$ solution.[4b] The formation mechanism involved the reduction of hardly soluble AgSCN in the aqueous solution by $NaBH_4$. However, the resulting silver nanoshells lacked stability in solution because of ready oxidation when exposed to ambient. This represents a major challenge for further engineering and practical applications.

In the present study, by adopting the one-pot synthesis method mentioned above,[4b] we prepared an Ag–Cu hollow nanoshell, which we believe is the first of its kind. The bimetallic nanoshells exhibited a rather uniform spherical structure, and were remarkably stable in solution for months at room temperature, in contrast to the monometallic Ag counterparts.[4b] Interestingly, the nanoscale cavity might be exploited for the encapsulation of selected molecules such as rhodamine 6G (R6G)[7] and phase transfer from water to apolar organic media by deliberate surface functionalization. In addition, the Ag–Cu nanoshells exhibited enhanced catalytic activity in the reduction of 4-nitroaniline by $NaBH_4$, as compared to solid Ag–Cu nanoparticles, likely due to ready accessibility of both the internal and external surfaces in the nanoshells for the catalytic reactions.

2. Results and Discussion

Stable Ag–Cu nanoshells were readily prepared by $NaBH_4$ coreduction of $AgNO_3$ and $Cu(NO_3)_2$ at the Ag:Cu initial feed

L. M. Chen, Dr. P. G. Hu, Y. Peng, J. E. Lu, M. D. Rojas-Andrade, Prof. S. W. Chen
Department of Chemistry and Biochemistry
University of California
1156 High Street, Santa Cruz, CA 95064, USA
E-mail: shaowei@ucsc.edu

DOI: 10.1002/ppsc.201600358

ratio of 3:1 in the presence of NaSCN, with cysteine being the capping ligands. The structures were first examined by transmission electron microscopic (TEM) measurements. From **Figure 1**A–C, one can see that indeed hollow nanoshells were successfully produced, with a mostly spherical shape. From the high-resolution TEM image in panel (D), the shells can be seen to exhibit well-defined lattice fringes, where the interplanar spacing of 0.237 nm is consistent with that of fcc Ag(111) crystalline planes (PDF card 65-2871), whereas the 0.253 nm spacing is in agreement with that of CuO(002) (PDF card 44-0706).[8] Interestingly, no lattice fringes were identified for metallic copper, indicating ready oxidation of copper into CuO in ambient. In addition, one can see that Ag and CuO formed segregated nanocrystalline domains rather than a homogeneous alloy, most likely because of their large lattice mismatch.[9] Statistical analysis based on more than 200 nanoshells showed that the outer diameter was averaged to be 57.2 ± 11.9 nm, with a shell thickness of 7.9 ± 1.6 nm, as manifested in the size histograms in panels (E) and (F), respectively, from which the hollow volume ratio was estimated to be ≈62% (v/v%).

The structures of the nanocomposites were then examined by X-ray diffraction (XRD) measurements (Figure S1, Supporting Information). Four major diffraction peaks can be identified at $2\theta = 38.2°$, 44.0°, 64.6°, and 77.2°, where the last three peaks might be ascribed to the diffraction of Ag (220), Ag (220), and Ag (311) crystalline planes, respectively, and the first peak likely arose from both Ag (111) and CuO (111). No other diffraction features were observed from CuO, possibly because of small crystallites or low crystallinity of CuO. Nonetheless, the XRD results suggest the formation of separate silver and copper phases, rather than an alloy structure, in the nanoshells. This is consistent with the results from TEM measurements (Figure 1D).

Similar hollow structures were observed with monometallic Ag nanoshells that were prepared in the same manner (Figure S2, Supporting Information), whereas without the addition of NaSCN, only solid Ag–Cu nanoparticles were obtained, which were markedly smaller with an average diameter of 3.79 ± 2.31 nm (Figure S3, Supporting Information). Notably, the Ag nanoshells were found to be rather defective (Figure S2, Supporting Information), as compared to the almost continuous shell structures observed with Ag–Cu nanoshells (Figure 1). This disparity may be accounted for by the formation mechanism of hollow nanostructures based on nanoscale Kirkendall effect, where the outward diffusion of inner ions and inward diffusion of reducing agent or the electrons injected by the reducing agent are known to play a significant role in determining the eventual structure.[10] In the synthesis of monometallic Ag nanoshells, the diffusion and nucleation of silver ions are too fast to form a complete shell.[11] However, with the addition of copper ions, the formation of continuous shells might be facilitated by the slower reduction and nucleation kinetics of copper, because of the more negative reduction potential. Consequently, reduction and subsequent nucleation of Cu likely occurred within the gaps between the silver crystalline domains. In such a reaction mechanism, formation of an Ag structural scaffold is a critical first step. Experimentally, it was found that when the Ag:Cu feed ratio was changed to 1:1, the structures of the eventual nanoshells were actually very close to the one prepared above at 3:1; whereas at a lower feed ratio of 1:3, no nanoshells were formed. This

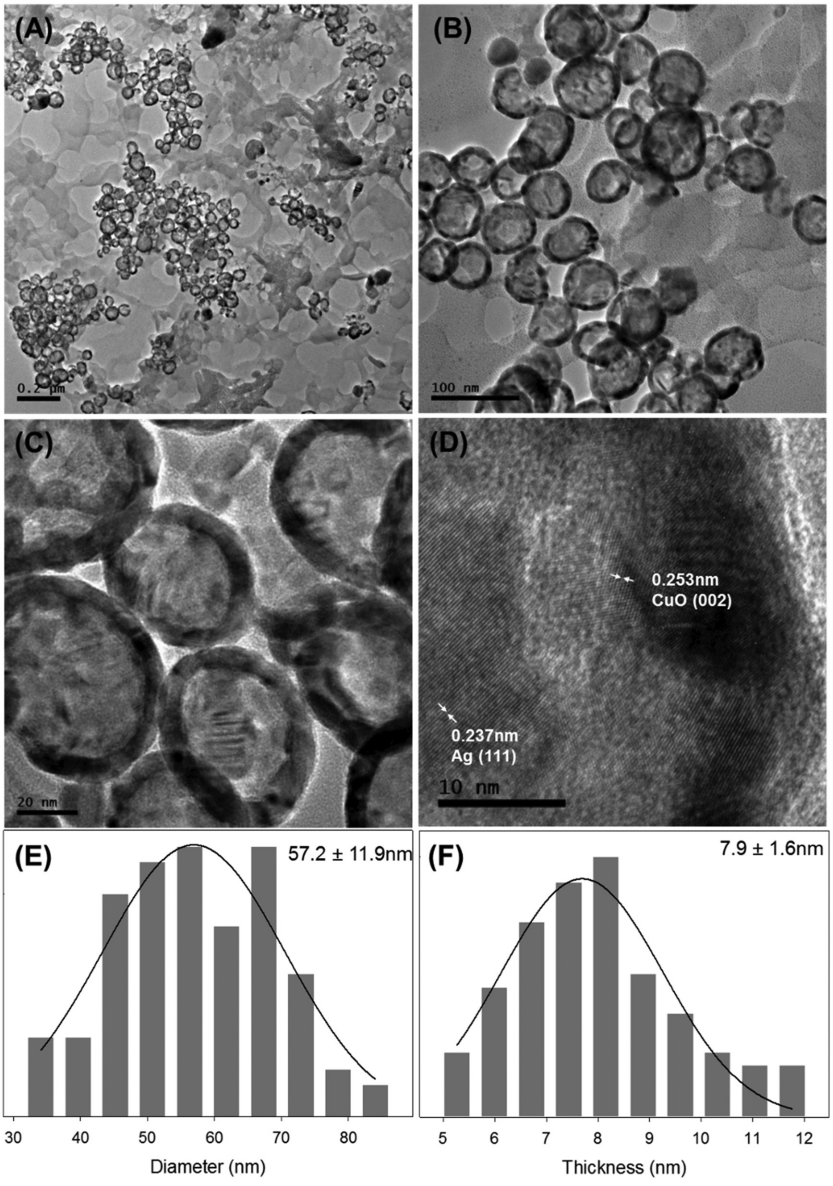

Figure 1. Representative TEM images of Ag–Cu nanoshells, where the scale bars are A) 200 nm, B) 100 nm, C) 20 nm, and D) 10 nm. The corresponding histograms of the nanoshell outer diameter and shell thickness are depicted in panels (E) and (F), respectively.

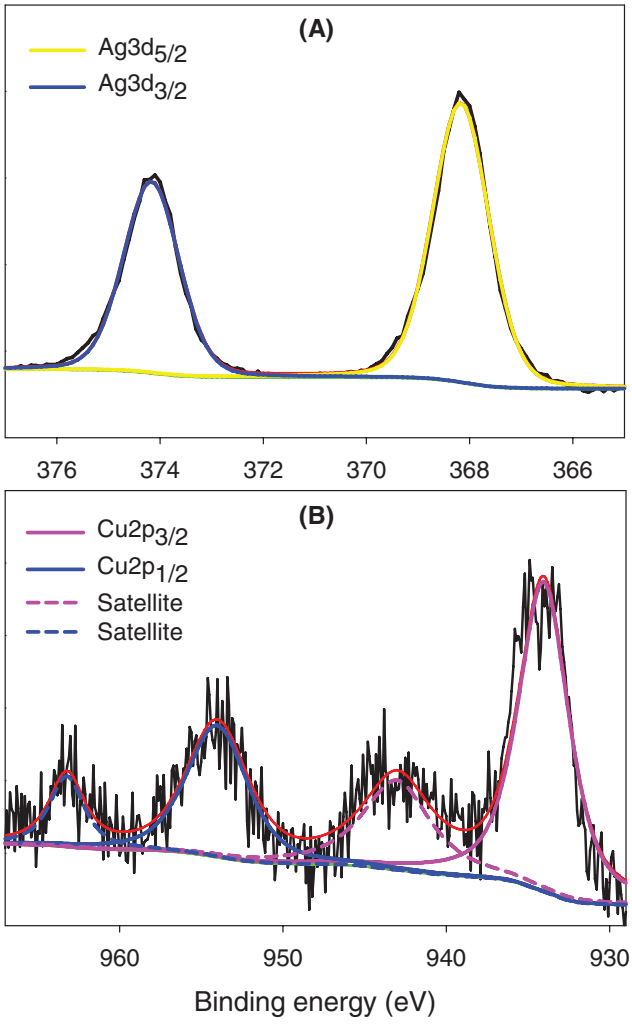

Figure 2. High-resolution XPS spectra of the A) Ag 3d and B) Cu 2p electrons in Ag–CuC12 nanoshells. Black curves are experimental data and colored curves are deconvolution fits.

suggests that the Ag:Cu feed ratio of 3:1 was optimal in the formation of stable nanoshell structures.

Further structural insights were obtained in X-ray photoelectron spectroscopic (XPS) measurements where the elemental compositions of the nanoshells were quantified. From the survey spectrum of the Ag–Cu nanoshells (Figure S4, Supporting Information), the Ag 3d and Cu 2p electrons can be readily identified at around 370 and 940 eV, respectively (along with S 2p at 163 eV and C 1s at 283 eV). The high-resolution scans of the Ag 3d and Cu 2p electrons are depicted in **Figure 2**. In panel (A), a doublet can be identified at 368.2 and 374.2 eV, consistent with the binding energies of the $3d_{5/2}$ and $3d_{3/2}$ electrons of metallic silver (identical to those of monometallic Ag nanoshells, Figure S5A, Supporting Information),[12] whereas the doublet at 934.2 and 954.2 eV in panel (B) may be assigned to the $2p_{3/2}$ and $2p_{1/2}$ electrons of Cu(II),[13] and the two satellite peaks at higher binding energies (943.2 and 963.4 eV) suggest the formation of CuO.[14] This is in good agreement with the results from TEM measurements (Figure 1). In addition, based on the integrated peak areas, the Ag:Cu atomic ratio was

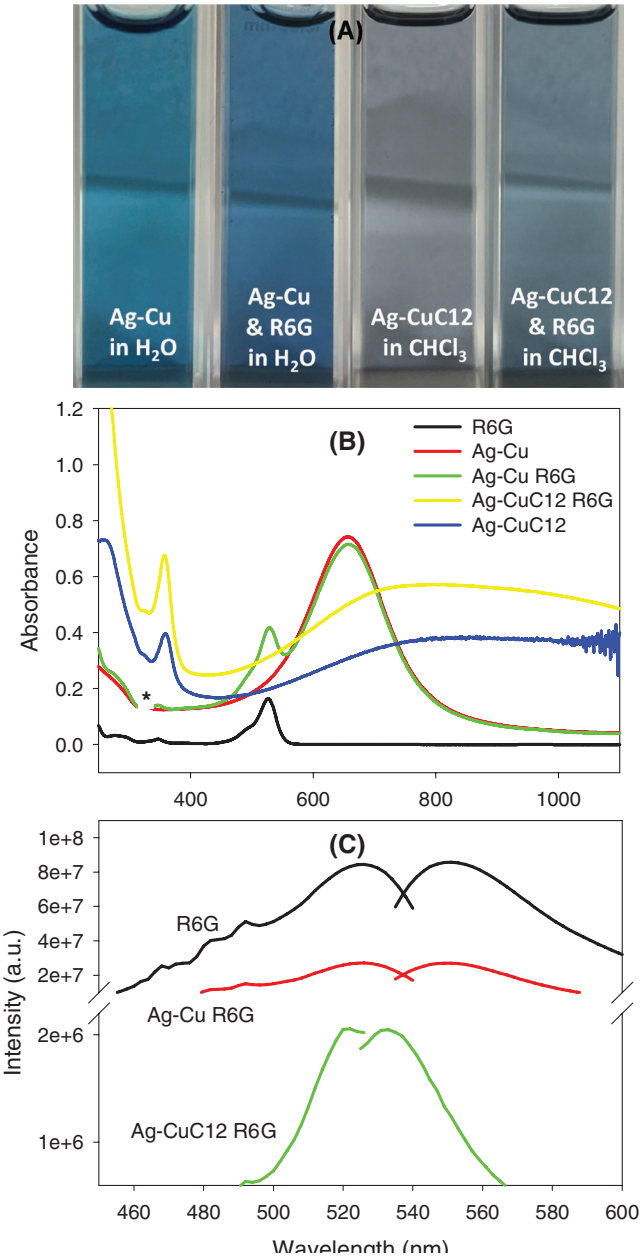

Figure 3. A) Photographs of Ag–Cu nanoshells in water, mixture of Ag–Cu nanoshells and R6G in water, Ag–CuC12 nanoshells in chloroform, and R6G encapsulated in Ag–CuC12 nanoshells in chloroform. B) UV–vis spectra of R6G in water (black curve), Ag–Cu nanoshells in water (red curve), mixture of R6G and Ag–Cu nanoshells in water (green curve), R6G encapsulated in Ag–CuC12 nanoshells in chloroform (yellow curve), and Ag–CuC12 in chloroform (blue curve). C) Photoluminescence spectra of R6G in water (black curve), Ag–Cu and R6G mixture in water (red curve), and R6G encapsulated in Ag–CuC12 nanoshells in chloroform (green curve).

calculated to be 3.02:1, almost identical to the molar feed ratio of the starting materials.

The optical properties of the Au–Cu nanoshells were then studied. From **Figure 3**A, it can be seen that the as-prepared Ag–Cu nanoshells exhibited a bright-blue color, with a well-defined absorption peak at 660 nm (red curve, Figure 3B). This can be assigned to the dipolar plasmon resonance of

the Ag–Cu nanoshells,[15] in contrast to that of solid Ag–Cu nanoparticles (380 nm, Figure S3C, Supporting Information) or monometallic Ag nanoshells (635 nm, Figure S5B, Supporting Information).[8a] Moreover, a small sharp peak (marked by an asterisk) at 325 nm can be observed, which is corresponding to the antisymmetric plasmon mode of the nanostructures. Overall, the UV–vis absorption characteristics are in agreement with those of hollow metal nanostructures.[4b]

To demonstrate the feasibility of the nanoshells as effective phase-transfer reagents, R6G dye was used as the illustrating probe (Figure 3). When a calculated amount of R6G was added into the aqueous solution of Ag–Cu nanoshells, in addition to the peak at 660 nm, a new prominent absorption band emerged at 525 nm, along with a shoulder at 499 nm (green curve, Figure 3B), which arose from the monomerization and dimerization of R6G molecules in aqueous solution, respectively.[16] Due to the combined contributions of R6G (pink) and Ag–Cu nanoshells (blue), the solution color became somewhat darker in blue (Figure 3A). The addition of a toluene solution containing 1-dodecanethiol (C12SH) into the above water solution led to surface functionalization of the nanoshells by the hydrophobic C12SH ligands (Ag–CuC12) through ligand-exchange reactions, and the nanoshells now became dispersible in $CHCl_3$ with a greenish blue color, bringing along R6G molecules trapped within the nanoshells to the organic phase (Figure 3A). The corresponding UV–vis absorption profile (yellow curve, Figure 3B) showed significant broadening of the dipolar surface plasmon resonance peak which red-shifted substantially to 700–900 nm (a red-shift to 360 nm was also observed with the antisymmetric plasmon resonance peak). This may be due to the higher refractive index of $CHCl_3$ (1.446) than that of water (1.333).[7,17] Note that without the loading of R6G, the Ag–CuC12 nanoshells in $CHCl_3$ showed a much lighter (bluish gray) color (Figure 3A), although the UV–vis absorption spectrum (blue cure, Figure 3B) looked similar.

The encapsulation of R6G into the Ag–Cu nanoshells was manifested in photoluminescence measurements. Figure 3C depicts the excitation and emission spectra of R6G in water, R6G mixed with Ag–Cu nanoshells in water, and R6G encapsulated in Ag–CuC12 nanoshells in $CHCl_3$. For the R6G solution in water (black curves), the excitation and emission peaks can be identified at 525 and 549 nm, respectively (R6G was also marginally soluble in $CHCl_3$ and exhibited almost identical peak positions).[7] Consistent photoluminescence characteristics were observed when R6G was added into the Ag–Cu nanoshells solution in water (red curves). Interestingly, when the Ag–Cu nanoshells were functionalized with C12SH and dispersed in $CHCl_3$, an apparent, though weaker, emission peak appeared at 532 nm at the excitation of 520 nm (green curves), suggesting that indeed R6G was entrapped within the Ag–Cu nanoshells, despite the absence of the characteristic absorption peaks of R6G at 525 and 499 nm in the UV–vis measurements (yellow curve, Figure 3B), most probably because of the low concentration of the nanoshells which contained only a small amount of R6G. The apparent disparity of the excitation and emission peak positions, as compared to those of free R6G and R6G mixed with Ag–Cu nanoshells in water, might be ascribed to the different chemical environments surrounding the R6G molecules.[18]

Furthermore, the cysteine-capped Ag–Cu nanoshells prepared above exhibited apparent catalytic activity toward the reduction of (yellow) 4-nitroaniline to (colorless) 4-phenylenediamine by $NaBH_4$ in water. 4-Phenylenediamine is an important component in engineering polymers, composites, hair dyes, and rubber antioxidant; and reduction of 4-nitroaniline to produce 4-phenylenediamine is a commonly used route.[19] Because of the marked color difference between the reactant and the product, the dynamics of this reduction reaction may be readily monitored by UV–vis absorption measurements. From **Figure 4**A, one can see that prior to chemical reduction (t = 0 min), the solution containing 4-nitroaniline and Ag–Cu nanoshells exhibited a dark green color, due to the combination of blue Ag–Cu nanoshells and yellow 4-nitroaniline, and with prolonging reaction time, the solution color gradually changed to blue and eventually resembled that of the Ag–Cu nanoshell solution alone, due to the reduction of 4-nitroaniline into colorless 4-phenylenediamine. Such an apparent colorimetric evolution can also be manifested in UV–vis measurements. From Figure 4B, one can see that at t = 0 min, the solution exhibited a well-defined absorption band at 380 nm due to the intermolecular charge transfer of 4-nitroaniline.[4a] At prolonging reaction times, the peak absorbance gradually decreased, and vanished altogether after 21 min; concurrently, two new absorption bands emerged at 235 and 300 nm, which exhibited a continuous increase of the peak intensities with reaction time, consistent with the effective reduction of 4-nitroaniline to 4-phen ylenediamine.[4a,19a,20] By contrast, with only $NaBH_4$ or with $NaBH_4$ and Ag–Cu solid nanoparticles, the reaction efficiency was markedly lower. For instance, after 21 min of reaction, only 10% of 4-nitroaniline was reduced with $NaBH_4$ alone, and 55% with $NaBH_4$ and Ag–Cu solid nanoparticles (Figure S6, Supporting Information), but for Ag–Cu nanoshells, 100% reduction of 4-nitroaniline was achieved. In fact, in comparison with results reported in recent literature with metal-based catalysts for 4-nitroaniline reduction (Table S1, Supporting Information), the performance of the Ag–Cu nanoshells is highly comparable, and in some cases even better, despite the use of a less amount of catalysts and a lower mole ratio of BH^-_4 to 4-nitroaniline in the present study.

Furthermore, one may notice a drastic blue-shift of the dipolar plasmon resonance of the Ag–Cu nanoshells during the reaction process (from 665 nm at t = 0 min to 615 nm at t = 21 min), along with an apparent increase of the peak absorbance and narrowing of the absorption band, most likely due to the injection of electrons by the reducing borohydride radicals in the solution.[21] Such electron accumulation on the nanoshell surface is critical for the catalytic reduction of 4-nitroaniline in the solution. This was manifested in the reaction kinetics which was analyzed by the variation of the peak absorbance at 380 nm with time. Figure 4C depicts the $\ln(C_t/C_0)$ versus time plot (green squares), where C_0 and C_t refer to the concentration (peak absorbance at 380 nm) of 4-nitroaniline at t = 0 and different reaction times, respectively. The good linearity suggests first-order reaction kinetics, and from the slope, the rate constant (k^{-1}) was estimated to 0.12 min^{-1}, about three times greater than that of Ag–Cu solid nanoparticles (0.04 min^{-1}, red

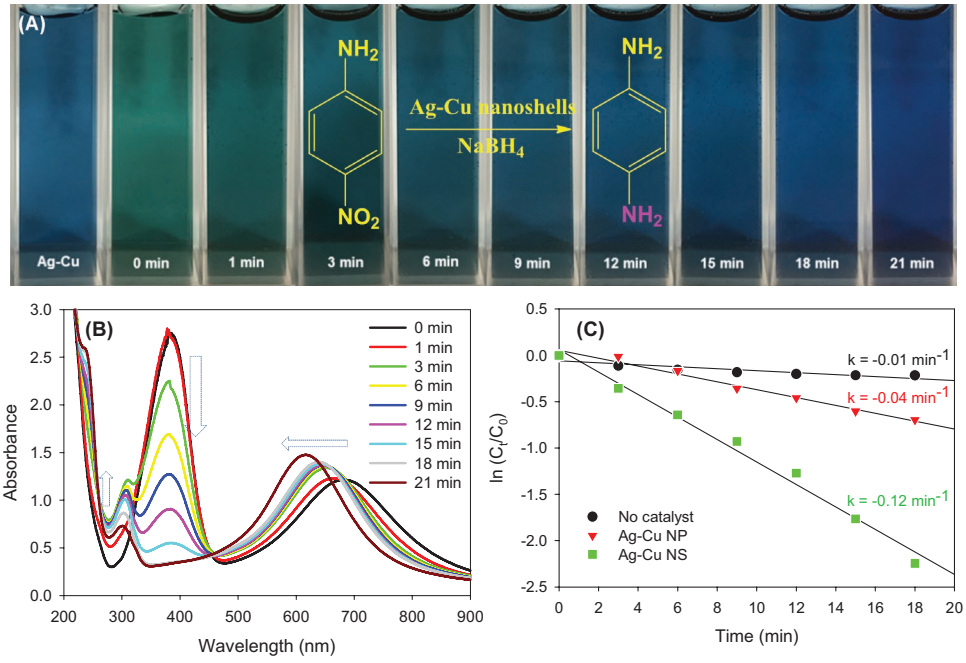

Figure 4. A) Photographs at different time intervals during the reduction of 4-nitroaniline by $NaBH_4$ using Ag–Cu nanoshells as the catalyst. B) UV–vis spectra of 4-nitroaniline reduced by $NaBH_4$ with Ag–Cu nanoshells as the catalyst at different reaction times (specified in figure legends), and C) the corresponding plots of $\ln(C_t/C_0)$ versus time, with no catalyst (black circles), Ag–Cu solid nanoparticles (red triangles), and Ag–Cu hollow nanoshells (green squares).

triangles) and 12 times that of the reaction without any catalyst (0.01 min^{-1}, black circles).

The recycling of the Ag–Cu nanoshells for the catalytic reduction of 4-nitroaniline was also tested by collecting the nanoshells by centrifugation at 6000 rpm for 15 min at the end of the experiment and using the nanoshells for repeat measurements. The catalytic activity was evaluated and compared for three more times. From Figure S7 (Supporting Information), it can be seen that the reductive conversion of 4-nitroaniline to 4-phenylenediamine after 18 min of reaction was 85.4%, 73.9%, 51.0%, and 54.9% for the first, second, third, and fourth cycle, respectively. This indicates that the Ag–Cu nanoshells can be easily recycled and reused with a high catalytic activity.

From the results presented above, one can clearly see that the morphologies of metal nanocrystals played a critical role in the catalytic reduction of 4-nitroaniline, which entails three major steps:[20c,22] (a) borohydride ions (BH^-_4) and nitro moieties chemically adsorb onto the metal surfaces; (b) hydrolysis of BH^-_4 leads to effective electron transfer to the metal surface and further to the nitro groups;[23] such an electronic relay mechanism helps overcome the kinetic barrier, and significantly improve the reaction kinetics;[20c] and (c) the reduction product 4-phenylenediamine desorbs from the metal surfaces. In the present study, the markedly higher reaction rate afforded by Ag–Cu nanoshells was likely due to the ready accessibility of both internal and external surfaces that facilitated the adsorption of reactant molecules and the accumulation of electrons injected from reducing reagents for the reduction of the nitro groups.

3. Conclusion

Stable Ag–Cu hollow nanoshells were prepared in aqueous solution by a facile one-pot process. The nanoscale cavity might be exploited for the encapsulation and phase transfer of target molecules, as illustrated by organic dye R6G as the molecular probe. The Ag–Cu nanoshells also exhibited enhanced catalytic activity toward the $NaBH_4$ reduction of 4-nitroaniline, as compared to Ag–Cu solid nanoparticles, most likely due to ready accessibility of both inner and outer surfaces of the nanoshells that facilitated adsorption and mass transport of the reactant and product molecules and interfacial electron-transfer dynamics.

4. Experimental Section

Chemicals: Silver nitrate ($AgNO_3$, Fisher Scientific), cupric nitrate ($Cu(NO_3)_2{\cdot}2.5H_2O$, Fisher Scientific), sodium thiocyanate (NaSCN, Fisher Science Education), sodium borohydride ($NaBH_4$, ≥98%, ACROS), sodium citrate dihydrate ($Na_3C_6H_5O_7{\cdot}2H_2O$, Fisher Scientific), R6G (99%, ACROS), 4-nitroaniline (98%, Alfar Aesar), L(+)-cysteine hydrochloride monohydrate (Cys, MCB), 1-dodecanethiol (C12SH, 96%, ACROS), and acetic acid (HOAc, Glacial, Fisher Scientific) were all used as received without any further purification. Solvents were purchased at the highest purity available from typical commercial sources and used as received. Water was supplied with a Barnstead Nanopure water system (18.3 MΩ cm).

Synthesis of Silver–Copper (Ag–Cu) Hollow Nanoshells: Silver–copper nanoshells were prepared by adopting a synthetic procedure reported in the literature for the preparation of monometallic Ag nanoshells.[4b] In brief, 0.5 mL of an aqueous solution of NaSCN (15×10^{-3} M) was diluted by 20 mL of Nanopure water to make a homogeneous solution,

and separately, 0.3 mL of a $AgNO_3$ aqueous solution (10×10^{-3} M) and 0.1 mL of a $Cu(NO_3)_2$ solution (10×10^{-3} M) (corresponding to an Ag:Cu molar feed ratio of 3:1) were added to 20 mL of Nanopure water. The NaSCN solution was then slowly added to the metal salt solution under magnetic stirring for 5 min to generate a blurry solution. Then 5 mL of a freshly prepared, cold $NaBH_4$ solution (1×10^{-3} M) was slowly added to the solution under constant stirring. Once the color of the solution started to turn bright blue (indicating the formation of Ag–Cu nanoshells), 0.1 mL of an aqueous solution of L(+)-cysteine (5×10^{-3} M) was immediately injected into the solution as protecting ligands. Excess ligands were removed by dialysis in Nanopure water for three days, affording purified cys-capped Ag–Cu hollow nanoshells.

As a control, monometallic silver nanoshells were prepared by using the same procedure[4b] except that no $Cu(NO_3)_2$ was added into the metal salt solution.

A second control was carried out with silver–copper solid nanoparticles. Experimentally, 0.75 mL of an $AgNO_3$ aqueous solution (10×10^{-3} M), 0.25 mL of a $Cu(NO_3)_2$ solution (10×10^{-3} M), and 0.01 mmol of sodium citrate dehydrate were added into 100 mL of Nanopure water, corresponding to an Ag:Cu molar feed ratio of 3:1; the solution was bubbled with nitrogen for 20 min, into which was then slowly added 12.5 mL of a freshly prepared, cold $NaBH_4$ solution (1×10^{-3} M). The appearance of a faint yellow color signified the formation of silver-rich nanoparticles. The solution was under magnetic stirring for 10 min before 0.25 mL of an aqueous solution of L(+)-cysteine (5×10^{-3} M) was added to the solution to stabilize the nanoparticles. The resulting nanoparticles were then purified by dialysis in Nanopure water.

Encapsulation of R6G Dye in Ag–Cu Nanoshells: Encapsulation of R6G inside the Ag–Cu nanoshells was carried out as follows. In a typical experiment, 200 µL of 1×10^{-3} M R6G was added into 40 mL of the aqueous solution of the nanoshells. After mixing under magnetic stirring for 4 h, 20 mL of toluene with 200 µL of 1-dodecanethiol was added to the above nanoshell solution, and the mixture was under magnetic stirring for 2 h. Then, 200 µL of HOAc was added into the solution. After stirring for another 15 min, the solution was left standing for 30 min, and the blue nanoshells were found at the water/organic interface. The nanoshells were then collected and purified with ethanol until the supernatant was colorless, which indicated the complete removal of free R6G molecules (and excess C12SH). The resulting C12SH-capped nanoshells were referred to as Ag–CuC12 (note that a small number of cysteine ligands remained on the nanoshell surface, as manifested in FTIR measurements, not shown).

Catalytic Reduction of 4-Nitroaniline by Ag–Cu Nanoshells: The experiment was carried out at room temperature (20 °C). Typically, 0.16 mg of the as-prepared cysteine-capped Ag–Cu nanoshells was dispersed in 14 mL of Nanopure water, along with 0.01 mmol of 4-nitroaniline. The color of the solution was found to change from bright blue to green-blue. 0.1 mmol of $NaBH_4$ dissolved in 200 µL of ice-cold water was then added as a reducing agent to the solution at room temperature. The UV–vis spectra of the solution were recorded at selected time intervals. At the end of the reduction reaction, the green-blue solution became bright blue again, signifying the full conversion of yellow 4-nitroaniline to colorless 4-phenylenediamine. To test the recyclability of the Ag–Cu nanoshells, the samples were collected by centrifugation at 6000 rpm for 15 min at the end of the experiment and used for repeat measurements under the otherwise identical conditions for a total of four cycles. Control experiments were carried out with solid Ag–Cu nanoparticles (also 0.16 mg) by using the same experimental procedure.

Structural Characterizations: The morphology and size of the metal nanostructures were characterized by TEM (Philips CM200 at 200 kV) studies. At least 200 nanoshells were analyzed to obtain a size distribution. XRD patterns were acquired with a Rigaku Americas Miniflex Plus diffractometer using Cu Kα radiation (λ = 1.5418 Å) within the range of 2θ = 10 to 80° at a scan rate of 2° min^{-1} with a 0.01° step size. UV–vis absorption spectra were collected with a Perkin-Elmer Lambda 35 spectrometer using a 1 cm quartz cuvette. Photoluminescence spectra were acquired with a PTI fluorescence spectrophotometer with a 450 W Xe lamp (Fluorolog, Jovin Yvon) and a close-cycle He cryostat (HC-2, APD Cryogenics). XPS spectra were recorded with a PHI 5400/XPS instrument equipped with an Al Kα source operated at 350 W and 10^{-9} Torr.

Supporting Information

Supporting Information is available from the Wiley Online Library or from the author.

Acknowledgements

This work was supported in part by the National Science Foundation (Grant No. DMR-1409396). TEM and XPS work was carried out at the National Center for Electron Microscopy and Molecular Foundry at the Lawrence Berkeley National Laboratory, which was supported by the US Department of Energy, as part of a user project.

Received: November 14, 2016
Revised: January 17, 2017
Published online:

[1] a) C. H. Cui, S. H. Yu, *Acc. Chem. Res.* **2013**, *46*, 1427; b) X. H. Tan, R. C. Jin, *Wiley Interdiscip. Rev.: Nanomed. Nanobiotechnol.* **2013**, *5*, 569; c) H. K. Sung, S. Y. Oh, C. Park, Y. Kim, *Langmuir* **2013**, *29*, 8978; d) C. H. Li, A. C. Jamison, S. Rittikulsittichai, T. C. Lee, T. R. Lee, *ACS Appl. Mater. Interfaces* **2014**, *6*, 19943.
[2] S. R. Mudshinge, A. B. Deore, S. Patil, C. M. Bhalgat, *Saudi Pharm. J.* **2011**, *19*, 129.
[3] a) M. R. Kim, J. Y. Kim, S. J. Kim, D. J. Jang, *Appl. Catal., A* **2011**, *393*, 317; b) H. X. Wu, P. Wang, H. L. He, Y. D. Jin, *Nano Res.* **2012**, *5*, 135; c) J. Zeng, Q. Zhang, J. Chen, Y. Xia, *Nano Lett.* **2010**, *10*, 30.
[4] a) W. M. Wu, S. J. Liang, Y. Chen, L. J. Shen, H. R. Zheng, L. Wu, *Catal. Commun.* **2012**, *17*, 39; b) S. Kado, S. Yokomine, K. Kimura, *RSC Adv.* **2014**, *4*, 10830; c) S. F. Xie, M. S. Jin, J. Tao, Y. C. Wang, Z. X. Xie, Y. M. Zhu, Y. N. Xia, *Chem. - Eur. J.* **2012**, *18*, 14974.
[5] F. Dong, W. Guo, S. K. Park, C. S. Ha, *Chem. Commun.* **2012**, *48*, 1108.
[6] Y. Choi, S. Hong, L. Liu, S. K. Kim, S. Park, *Langmuir* **2012**, *28*, 6670.
[7] F. M. Zehentbauer, C. Moretto, R. Stephen, T. Thevar, J. R. Gilchrist, D. Pokrajac, K. L. Richard, J. Kiefer, *Spectrochim. Acta, Part A* **2014**, *121*, 147.
[8] a) H. J. Jiang, K. S. Moon, C. P. Wong, *Proc. 10th Int. Symp. Adv. Packag. Mater.: Processes, Prop., Interfaces,* **2005**, *173*; b) P. G. Hu, Y. Song, L. M. Chen, S. W. Chen, *Nanoscale* **2015**, *7*, 9627; c) D. Q. Gao, J. Zhang, J. Y. Zhu, J. Qi, Z. H. Zhang, W. B. Sui, H. G. Shi, D. S. Xue, *Nanoscale Res. Lett.* **2010**, *5*, 769.
[9] a) P. A. Huttunen, J. Makinen, A. Vehanen, *Phys. Rev. B* **1990**, *41*, 8062; b) M. Tsuji, S. Hikino, R. Tanabe, M. Matsunaga, Y. Sano, *CrystEngComm* **2010**, *12*, 3900; c) K. S. Tan, K. Y. Cheong, *J. Nanopart. Res.* **2013**, *15*, 1537.
[10] A. Ben Moshe, G. Markovich, *Chem. Mater.* **2011**, *23*, 1239.
[11] W. S. Wang, M. Dahl, Y. D. Yin, *Chem. Mater.* **2013**, *25*, 1179.
[12] a) S. X. Dai, X. T. Zhang, T. F. Li, Z. L. Du, H. X. Dang, *Appl. Surf. Sci.* **2005**, *249*, 346; b) K. Mansikkamaki, U. Haapanen, C. Johans, K. Kontturi, M. Valden, *J. Electrochem. Soc.* **2006**, *153*, B311.
[13] a) S. W. Lee, Y. S. Lee, J. Heo, S. C. Siah, D. Chua, R. E. Brandt, S. B. Kim, J. P. Mailoa, T. Buonassisi, R. G. Gordon, *Adv. Energy Mater.* **2014**, *4*, 1301916; b) J. M. Knight, R. K. Wells, J. P. S. Badyal, *Chem. Mater.* **1992**, *4*, 640.

[14] Y. K. Hsu, C. H. Yu, Y. C. Chen, Y. G. Lin, *RSC Adv.* **2012**, *2*, 12455.
[15] P. Tuersun, X. E. Han, *Appl. Opt.* **2013**, *52*, 1325.
[16] A. P. Rao, A. V. Rao, *Sci. Technol. Adv. Mater.* **2003**, *4*, 121.
[17] a) Y. Hu, R. C. Fleming, R. A. Drezek, *Opt. Exp.* **2008**, *16*, 19579; b) M. R. Rasch, K. V. Sokolov, B. A. Korgel, *Langmuir* **2009**, *25*, 11777.
[18] I. Trenkmann, S. Bok, V. R. Korampally, S. Gangopadhyay, H. Graaf, C. von Borczyskowski, *Chem. Phys.* **2012**, *406*, 41.
[19] a) M. Abbas, S. R. Torati, C. Kim, *Nanoscale* **2015**, *7*, 12192; b) M. C. Gennaro, P. L. Bertolo, E. Marengo, *J. Chromatogr.* **1990**, *518*, 149.
[20] a) Q. Zhou, G. Z. Qian, Y. Li, G. Zhao, Y. W. Chao, J. W. Zheng, *Thin Solid Films* **2008**, *516*, 953; b) K. Sharma, V. Bhalla, M. Kumar, *RSC Adv.* **2014**, *4*, 53795; c) P. S. Rathore, R. Patidar, T. Shripathi, S. Thakore, *Catal. Sci. Technol.* **2015**, *5*, 286.
[21] a) A. Henglein, P. Mulvaney, T. Linnert, *Faraday Discuss.* **1991**, *92*, 31; b) T. Ung, M. Giersig, D. Dunstan, P. Mulvaney, *Langmuir* **1997**, *13*, 1773.
[22] P. Herves, M. Perez-Lorenzo, L. M. Liz-Marzan, J. Dzubiella, Y. Lu, M. Ballauff, *Chem. Soc. Rev.* **2012**, *41*, 5577.
[23] C. F. Hsia, M. Madasu, M. H. Huang, *Chem. Mater.* **2016**, *28*, 3073.
[24] H. P. Xia, W. K. C. Cheung, S. S. Ng, X. C. Jiang, S. S. Jiang, J. Sze, G. K. K. Leung, G. Lu, D. T. M. Chan, X. W. Bian, H. F. Kung, W. S. Poon, M. C. Lin, *J. Biol. Chem.* **2012**, *287*, 9962.
[25] A. Shaabani, Z. Hezarkhani, M. K. Nejad, *RSC Adv.* **2016**, *6*, 30247.